Engineering Structures 283 (2023) 115927

Contents lists available at ScienceDirect

Engineering Structures

journal homepage: www.elsevier.com/locate/engstruct

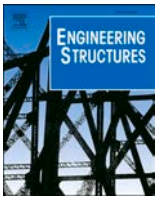

Calibration of concrete damaged plasticity materials parameters for tuff masonry types of the Campania area

Elide Nastri, Michela Tenore, Paolo Todisco *

Department of Civil Engineering, University of Salerno, Fisciano, SA, Italy

ARTICLE INFO

Keywords:
Masonry
FEM
Macromechanical models
Failure criteria
Concrete damage plasticity

ABSTRACT

The masonry buildings represent the largest portion of the Italian building heritage considering that about eighty percent of buildings is made of different kind of masonry. Italian cities are characterized by the presence of numerous masonry buildings of historical and architectural value. It is possible to find a large variety of building techniques and constructional material leading to different masonry structures that need to be precisely characterized as regards the mechanical behaviour. In this paper, the calibration of the materials parameter for an adequate modelling of typical tuff masonry constructive systems spread in Campania region is given. The calibration has been developed reproducing, by FEM analysis, real compression tests performed in displacement control available in literature. In particular, reference is made to masonry with regular ashlars, listed tuff masonry and chaotic tuff masonry. The FEM analyses have been carried out considering the "Concrete Damaged Plasticity" failure criteria. Moreover, the modelling of a wall subjected to horizontal actions has been investigated with reference to solid brick elements and shell to analyse if there is any shape factor affecting the different response. It can be pointed out that the analytical model used for the calibration of uniaxial tension and compression curves shows great adaptability and versatility for each type of masonry.

1. Introduction

The masonry buildings constitute a large portion of the Italian building heritage as about the eighty percent of buildings is made of different kind of masonry. According to the 2011 ISTAT census [1], the number of residential buildings in load-bearing masonry is about the 57.24% of residential buildings in Italy, among which, the ones dating back to prior than 1919 are in a poor state of preservation. Italian cities, big or small, are characterized by the presence of numerous masonry buildings of great historical and architectural value. The masonry is a not homogenous material as its characteristics depends on the mortar, stones, texture and constructive technique which depends on the period and the availability of material in the area of the erection. In a relatively small area, we can find a large variety of building techniques and constructional material leading to different masonry structures that need to be detailly characterized in terms of mechanical behaviour. Moreover, each historical period has its peculiar constructive technique. Despite of this large variety, existing masonry have in common the medium–high level of vulnerability against seismic actions [2].

The catastrophic seismic events of the last decades among which we recall the most impactful, namely the Irpinia Earthquake of 1980, the San Giuliano di Puglia earthquake of 2002, and the more recent event occurred in the Central Italy have produced an impact in economic terms and human lives. It is clear how, even without further reference to numerical data, many culturally relevant buildings, such as churches, important residential buildings and public buildings in Italy are particularly prone to be furtherly damaged by earthquakes and they have already experienced several seismic events during their life.

This means that a comprehensive modelling of the masonry structures as possible as more compliant with the constructive detail and materials is of paramount importance for the evaluation of the seismic vulnerability of the building.

It is generally possible to distinguish two types of numerical approaches for the masonry modelling: finite element modelling, and discrete element modelling. In the first case, the masonry is discretized into two-dimensional or three-dimensional finite elements. In the case of regular masonry, it is possible to modelling through a detailed strategy defined as "micro-modelling" [3,4,5,6,7,8,9], which can be in turn distinguished into detailed and simplified. The detailed micro-modelling aims to exactly reproduce the geometry of the structure, going to

* Corresponding author.
E-mail address: ptodisco@unisa.it (P. Todisco).

https://doi.org/10.1016/j.engstruct.2023.115927
Received 9 November 2022; Received in revised form 19 January 2023; Accepted 28 February 2023
Available online 13 March 2023

distinguish every stone element and every joint, while the simplified one extends the dimension of the stone elements up to the middle line of the mortar joints, to employ a continuous and homogeneous model for the stone elements and to describe the behaviour of the joints by means of interface surfaces. For regular masonry, it is always possible to follow the "macro-modelling" approach [10,11,12,13,14,15,16]. In this case the masonry is reduced into a single continuous homogeneous material, without distinguishing the stone elements and the single mortar joints. The discrete elements modelling [17,18,19,20,21], instead, is used in the case in which we deal with very irregular masonry, for which the modelling of the single elements would involve an excessive burden. In this case, the stone elements are understood as bodies connected by interface surfaces. In the case of structures subject to modest stress and deformation states, the stone elements can be modelled as rigid, otherwise they are assumed to be deformable. In the case of buildings consisting of walls mutually connected, at different heights, by decks, it is possible to define a type of simplified macro-element modelling. It allows a simulation of the experimentally measured behaviour and of the observed crack patterns after major seismic events, without committing significant errors.

The Finite Element Modelling (FEM) [22,23,24,25,26], allow to discretize the continuum using subdomains and through the choice of some points, called nodes, on the boundary or within the finite elements. The FE can have different shapes, quadrangular or triangular, and have a different number of nodal points. In general, it is good to use regular shaped elements, so squares and equilateral triangles rather than rectangles or thin triangles, and it is good to account for many nodes in areas where the maximum stresses are expected to be located. In addition, the FEM can be limited to a simplified equivalent homogeneous model, or it can be pushed to a more accurate modelling, in which mortar and bricks are modelled separately. In general, the choice of the model must be made according to the structural type and depending on the complexity and availability of data. It is necessary to find the correct compromise between reliability of the model, and therefore more or less precise approximation of the reality, and calculation times that do not involve a burden too heavy. Too much complex models, sometimes with useless and harmful sophistications, can incur to errors during the phase of modelling and computation, with the consequent developed of inaccurate results. It results preferable to use simpler models but able to represent in well approximated way the reality, thanks to the correct calibration of the parameters.

In this paper, the calibration of the parameter for an adequate modelling of typical tuff masonry constructive systems spread in Campania region (Italy) is reported [27,28,29,30]. Reference is made to masonry with regular ashlars and listed tuff masonry [31]-[32]. Experimental tests under compressive and tensile load have been simulated. Moreover, to understand the behaviour of such masonry types under horizontal actions the experimental tests on a real scale wall have been simulated with their original material by using both solid brick and shell elements to understand the difference in the response due to the different modelling. After the calibration procedure, the materials investigated in this paper have been applied to the same wall. The set parameters can be used for the modelling of the masonry walls to be used in the building modelling.

In Section 2 the selected masonry typology and the motivation regarding their choice are reported. In Section 3 the FEM modelling through Concrete Damaged Plasticity (CDP) is described while in Section 4 the analytic model for the definition of the tensile and compressive behaviour is reported. The calibration of the macro-mechanical behaviour of the selected masonry is described in Section 5 and detailed in the Appendix. In Section 6 the calibration of the model behaviour using both shell and brick elements is described. The Conclusions sections resumes the main outcomes of the paper.

The main results obtained concern the calibration of the parameters for the definition of uniaxial tension and compression curves (input data for CDP failure criterion) in accordance with the Guo model. The parameters obtained for CDP failure criterion can be used to analyse the numerous existing buildings made with the considered materials. In addition, a comparison was made between "shell" and "brick" models for both compression and shear actions. The "shell" model did not show any differences in terms of accuracy but guarantees a quicker computation.

2. Investigated masonry typology

Masonry with regular ashlars is one of the most common constructive techniques spread in all the Campania region and in the south of Lazio region dating back to XVIII century. They are usually characterized by rows of tuff blocks clearly identifiable in regular ashlars. This kind of masonry is often of wide thickness, and it is characterized by two external panels with interposed material used to connect both the external panels. It is mainly in yellow tuff, however, in many areas it is made of grey tuff which is stiffer and more resistant than the yellow one.

In this paper four typical typologies of tuff masonry have been investigated. Their chronological affiliation ranges in a period going from the XVI and XX century and they are largely spread in all the Campania region and in the south of Lazio region. If in the Neapolitan area there is a large use of yellow tuff, in other parts of Campania region the grey tuff is more spread. However, the technological features are almost the same.

Metrological research carried out on the tuff in Neapolitan area have pointed out that is possible to mainly identify four constructive types which can be defined by homogeneous chronological, morphological, and dimensional parameters. Such masonries are [31,32]:

- *Cantieri* masonry, widespread in the XVI and XVII centuries which is characterised by the piling up of irregular broken stone, layered on tick bed of conglomerate. The main characteristic of this constructive technique is that the layer of mortar is clearly identifiable constituting the so-called "cantieri". Each "cantieri" layer was about 55 cm height. Some examples of application of "cantieri" masonry are the Church of S. Caterina a Formiello (1501–1514), the "Palazzo Don-n'Anna" in Posillipo (1642–1644) and the foundations of "Quartieri Spagnoli" also in Naples. In Fig. 1 and Fig. 2 some examples of Cantieri masonry made of grey tuff are reported.
- *Bozzette* masonry, dating back to XVIII century. They were made by the use of roughly worked elements of the same size constituting layers of about 13 cm of height. Some examples of bozzette masonry are the Royal palace of Portici in Naples (accomplished in 1973). In Fig. 3 and Fig. 4 two examples of "bozzette" masonry made of yellow and grey tuff are reported.

Fig. 1. Perimetral walls of the Virginian Monks Coventry in Penta di Fisciano (SA), Italy. (Second half of XVII century).

Fig. 2. Perimetral walls of the Coventry of Carmelitan nuns in Fisciano (SA), Italy. (Second half of XVII century).

- *Blocchetti a filari* masonry used in XIX century and first half of XX century made of blocks accurately squared of about 20–25 cm of height. This constructive typology is used to build several buildings and can be considered the constructive typology more spread for what regards the ancient masonry in Neapolitan area. Some examples are the psychiatric hospital L. Bianchi in Naples. In Fig. 5 and Fig. 6 some examples of "blocchetti a filari" masonry are reported.
- *Listed masonry*, used in XVIII and XIX centuries. They are made by bozzette or blocchetti masonry of tuff with interlocked layers of very thin clay brick. The layers of bricks can go to one to four layers. Some examples of listed masonry is a portion of the abside of the Cathedral of Naples. In Fig. 7 and Fig. 8 an example of listed masonry with one layer and two layers, respectively, are reported.

The photos in Figs. 1–8 are snap by the authors in the area surrounding the University of Salerno (Fisciano), thus testifying how spread are such kind of masonry typology which are not limited to building of high importance or strategical but also to the common buildings. The main features of the analysed masonry, i.e. name, age period and schematic drawing are reported in Table 1.

3. Finite element modelling: Concrete Damaged Plasticity

The four typical typologies of tuff masonry have been investigated through the Concrete Damaged Plasticity (CDP) failure criterion, a continuous model based on two main failure mechanisms, namely the *tensile cracking* and *compressive crushing* [33,34].

Fig. 3. Tower bell of St. Martino church in Lancusi di Fisciano (SA), Italy. (XVIII century).

The evolution of the damage and consequently the failure surface is governed by two variables, i.e. the plastic deformation in traction ε_t^p and in compression ε_c^p (Fig. 9). The tensile d_t and compressive d_c damage functions can be used to define the stress–strain relations in tension and in compression:

$$\sigma_t = (1 - d_t)E_0\left(\varepsilon_t - \varepsilon_t^p\right) \tag{1}$$

$$\sigma_c = (1 - d_c)E_0\left(\varepsilon_c - \varepsilon_c^p\right) \tag{2}$$

Fig. 4. City hall of Mercato San Severino (SA), Italy. (XVIII century).

Fig. 5. Baronal Palace of De Falco family, Fisciano (SA) Italy. (XIX century).

Fig. 6. Copper foundry, Fisciano (SA), Italy. (first half of XX century).

with d_t and d_c equal to 0 in case of zero damage and equal to 1 in case of total damage. The reduced elastic modulus E is given by $E = (1 - d_t)E_0$ and $E = (1 - d_c)E_0$ in tension and compression, respectively, where E_0 is the initial elastic modulus.

In the case of uniaxial cyclic loading, the opening and closing of the micro-cracks and their interaction play a fundamental role. It is experimentally observed that there is a recovery of elastic stiffness in the moment of inversion of the stress sign and it is greater in the case of transition from traction to compression. In this case, the reduction of the elastic modulus is related to the variable d which is a function of the previously described damage parameters d_t and d_c, and of the reversal functions s_t and s_c, depending on the stress state. In particular, they allow to specialize the relation as a function of the passage from positive to negative stresses or vice versa and using also the weight factors w_t and w_c representing the extent of the recovery of stiffness in the compression-traction and traction-compression switching (Fig. 10).

The elastic modulus E can be expressed by the following relation:

$$E = (1 - d)E_0 \tag{3}$$

The reduction facto $(1 - d)$, is valid for both tension ($\sigma_{11} > 0$) and compression $\sigma_{11} < 0$ and it can be furtherly written as:

$$(1 - d) = (1 - s_t d_c)(1 - s_c d_t) \tag{4}$$

where the stress reversal functions) s_t and s_c are:

$$s_t = 1 - w_t r^*(\sigma_{11}); \quad 0 \le w_t \le 1 \tag{5}$$

$$s_c = 1 - w_c(1 - r^*(\sigma_{11})); \quad 0 \le w_c \le 1 \tag{6}$$

where r^* is a step function dependent on the sign of the tensions:

$$r^*(\sigma_{11}) = \begin{cases} 1 if \ \ \sigma_{11} > 0 \\ 0 if \ \ \sigma_{11} < 0 \end{cases} \tag{7}$$

In multiaxial cases, the relationships are generalized by replacing the step function $r^*(\sigma_{11})$ with the pluriaxial weight factor $r(\sigma)$ and applied to

Fig. 7. Pillar of Madonna del Fieno Chapel, Fisciano (SA), Italy. (XIX century).

the initial elasticity matrix $\bar{\bar{D}}_0$ according to the relation:

$$(1-d)\bar{\bar{D}}_0\left(\underline{\varepsilon}-\underline{\varepsilon}_p\right) \tag{8}$$

The ABAQUS software foresees the definition of the uniaxial behaviour in tension as a function of the cracking strain ε_t^{ck}, defined as the difference between the total deformation and the elastic deformation corresponding to a material without damage ($d_t = 0$). In analytical terms it results:

$$\varepsilon_t^{ck} = \varepsilon_t - \varepsilon_{0t}^{el} \tag{9}$$

with $\varepsilon_{0t}^{el} = \sigma_t/E_0$. The cracking strain can be converted into plastic strain according to:

$$\varepsilon_t^{p} = \varepsilon_t^{ck} - \frac{d_t}{(1-d_t)}\frac{\sigma_t}{E_0} \tag{10}$$

while the uniaxial behaviour in compression, can be defined as the difference between the total deformation and the elastic deformation corresponding to material without damage ($d_t = 0$):

$$\varepsilon_c^{in} = \varepsilon_c - \varepsilon_{0c}^{el} \tag{11}$$

where ε_c^{in} is the inelastic strain and ε_{0c}^{el} is the deformation of the undamaged material computed as.$\varepsilon_{0t}^{el} = \sigma_t/E_0$

The inelastic strain is subsequently converted into plastic strain according to:

$$\varepsilon_c^{p} = \varepsilon_c^{in} - \frac{d_c}{(1-d_c)}\frac{\sigma_c}{E_0} \tag{12}$$

The data are implemented in terms of $\sigma_t - \varepsilon_t^{ck}$ and $\sigma_c - \varepsilon_c^{in}$ and the damage parameters d_t and d_c, must be reported with the same intervals of $\varepsilon_t^{ck}, \varepsilon_c^{in}$ provided for the tensions.

The yielding or failure function f is provided as a function of the maximum effective principal stress while a Drucker-Prager function has been chosen as the flow rule. As regards the damage functions d_t and d_c, they can be obtained through experimental or analytical curves of proven validity according to the relations:

$$d_t = 1 - \frac{E_t}{E_0} \tag{13}$$

$$d_c = 1 - \frac{E_c}{E_0} \tag{14}$$

where E_t and E_c represent the elastic modulus values obtained through load-unload tests with load values greater than σ_{t_0} (yield strength) in tension and σ_{c_u} (ultimate load) in compression. Through the evolution of the elastic modulus, it will therefore be possible to derive the damage functions (Fig. 11). In a simplified way, reference can be made to the evolution of tensions through the following relations:

$$d_t = 1 - \frac{\sigma}{\sigma_{t_0}} \tag{15}$$

Fig. 8. House in Via Sabatini 16, Fisciano (SA), Italy. (probably XIX century).

Table 1
Scheme of the selected masonry typology with the reference of the age period and name.

Name	Age	Drawing
Cantieri	XVI and XVII centuries	
Bozzette	XVIII century	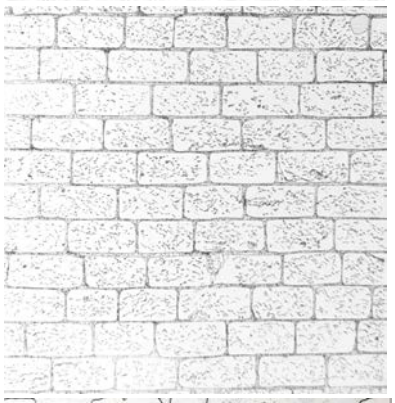
Blocchetti a filari	XIX century and first half of XX century	
Listed	XVIII and XIX centuries	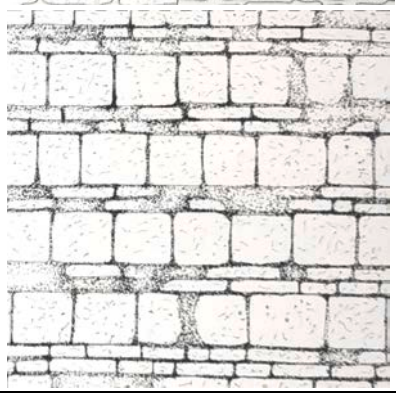

$$d_c = 1 - \frac{\sigma}{\sigma_{c_u}} \tag{16}$$

4. Analytic model for the definition of the compressive and the tensile behaviour

The CDP model [35,36] is the most suitable for the analysis of wall panels, especially for the control of cracks, being a model in which the evolution of the failure domain and therefore of the parameters that govern its behaviour, is linked to the level of damage due to the plastic deformation ε_p. In particular, in this model the cohesion is linked to the formation of cracks and consequently to the plastic deformation.

An accurate discussion about the CDP model and the comparison with different models is reported in [10]. The characterization of the model takes place through the implementation of uniaxial tension and compression $\sigma - \varepsilon$ diagrams for which numerous publications on experimental tests are available in the literature, through which it is possible to carry out a direct control on the adherence of the results. analytics to real behaviour.

The uniaxial constitutive links were reconstructed according to the model proposed by Guo [37].

This model has been selected after analysing several papers concerning the calibration of uniaxial tensile and compression curves. In particular, both for masonry [34,35] and concrete [36], reference is made to the Guo model as a choice that allows high adaptability. Moreover, these characteristics have already been confirmed by the analyses carried out in [10]. This model is capable to represent as continuous function the uniaxial tension and compression curves required by Abaqus software. In this way, through the knowledge of only the elastic modulus, the secant modulus, the maximum stress and the parameters calibrated in this work, it is possible to catch the uniaxial behaviour of the considered material.

In the constitutive models of CDP [35,36,37], the elastic deformation ε_{el} and the plastic deformation ε_{pl}, are calculated separately and then added together, to obtain the total deformation ε. The elastic deformation depends on the elastic modulus and the Poisson's modulus of the material, while the inelastic deformation is obtained through the stress-deformation curves.

The formulations for the construction of the behaviour curve of the material under a uniaxial compression are for the (Fig. 12):

- Elastic region:

$$\sigma_c = E_{cm} \cdot \varepsilon \tag{17}$$

where E_{cm} is the initial modulus of elasticity (stress of 0.3–0.8 f_{bm}) and ε is the generic deformation.

- Inelastic region:

$$\sigma_c = f_{bm}\left[\alpha_a x + (3 - 2\alpha_a)x^2 + (\alpha_a - 2)x^3\right] x \leq 1 \tag{18}$$

$$\sigma_c = f_{bm} \cdot \frac{x}{\alpha_d (x-1)^2 + x} x > 1 \tag{19}$$

where:

$$x = \frac{\varepsilon}{\varepsilon_{c1}}, \alpha_a = \frac{E_{cm}}{E_{c1}}, 0.4 \leq \alpha_d \leq 4 \tag{20}$$

and where E_{c1} is the secant modulus corresponding to the maximum stress. The parameter α_d affects the shape of the descendant branch of the curve (Fig. 13) and must be calibrated through experimental tests.

As regards the uniaxial tensile behaviour, an elastic region and an inelastic region are distinguished based on Guo. The σ-ε constitutive law is described by the following relations (Fig. 14):

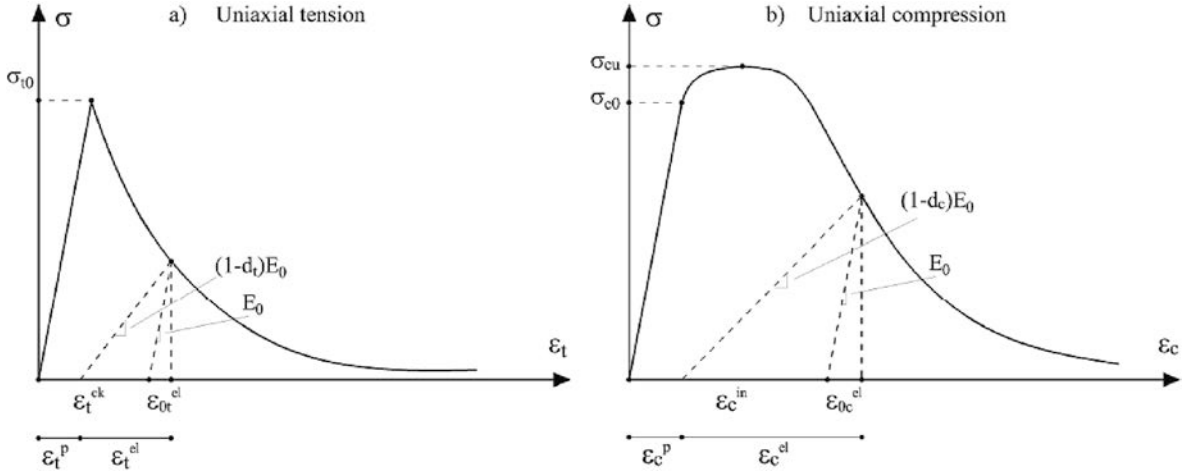

Fig. 9. Concrete Damaged Plasticity in ABAQUS, uniaxial model for tension and compression.

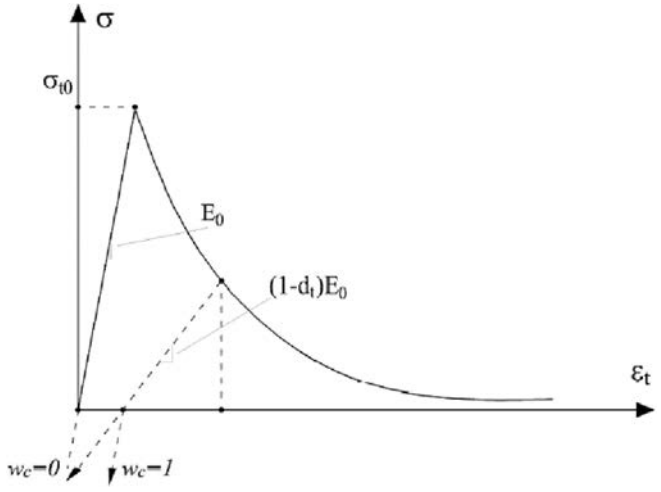

Fig. 10. Concrete Damaged Plasticity in ABAQUS, load reversal from tension to compression.

- Elastic region:

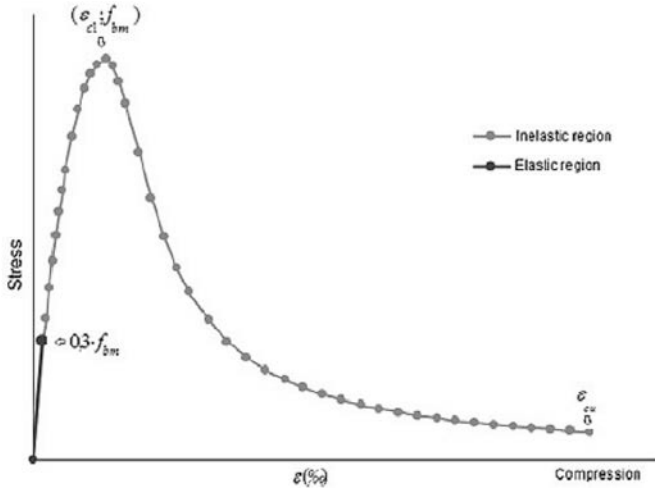

Fig. 12. Uniaxial compression model by Guo.

$$\sigma_t = E_{cm} \cdot \varepsilon \tag{21}$$

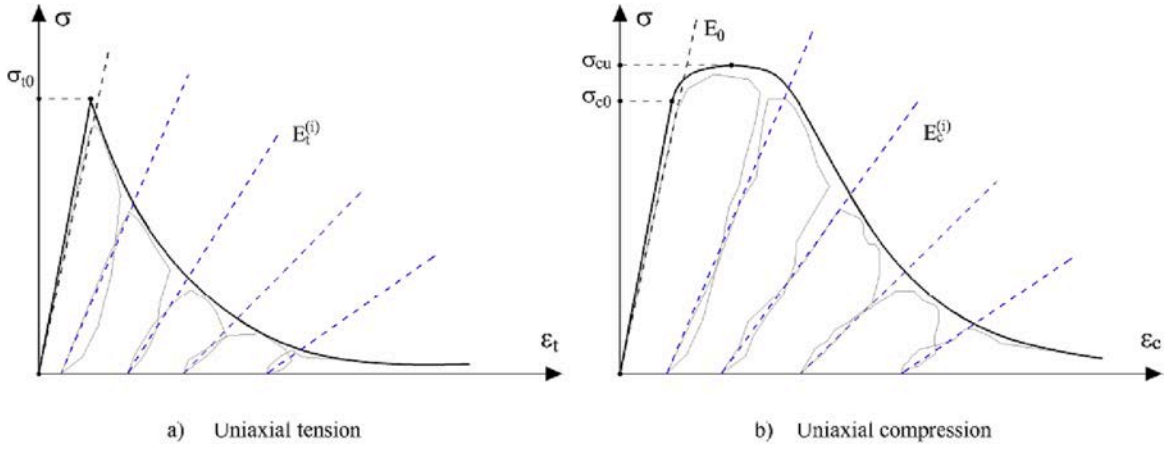

Fig. 11. Concrete Damaged Plasticity in ABAQUS, evolution of the elastic modulus E in tension and in compression.

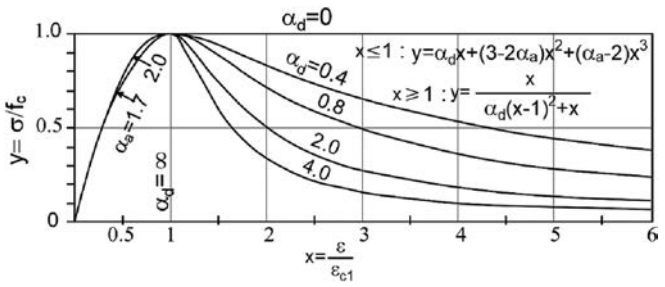

Fig. 13. Effect of the α_d parameter on the descendant part of the curve.

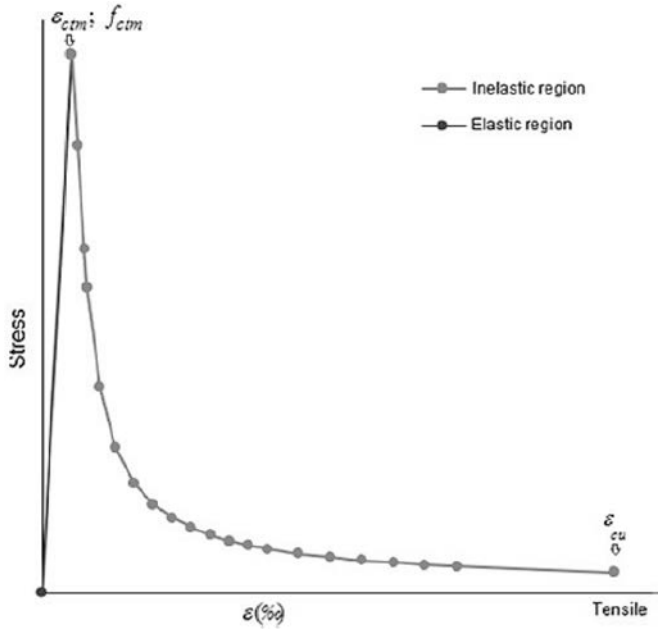

Fig. 14. Uniaxial tension model.

where E_{cm} is the initial tangent modulus of elasticity and ε is the generic deformation.

- Inelastic region:

$$\sigma_c = f_{btm} \cdot \frac{x}{\alpha_t (x-1)^{1.7} + x} \tag{22}$$

where $\alpha_t = 0.312 f_{btm}$ and f_{btm} is the tensile strength of the material

$$x = \frac{f_{btm}}{E_{cm}} \tag{23}$$

5. Calibration of the material parameters according to the analytical model

5.1. Quasi-static explicit analysis in FEM models

The Finite Element Method (FEM) subdivides the general problem into many sub-problems, which are simpler to solve, and which require to be solved by either an implicit or an explicit type of analysis. Both types of analysis are expressed through ordinary differential equations and partial derivative differential equations, both dependent on the time variable, which may be linear or nonlinear. In most structural problems, the nonlinearity is due to one of these three aspects: material, geometry, or boundary conditions. To understand the difference between explicit and implicit analysis, it must be stated that while implicit methods find a solution by solving equations involving both the current state of the system and the one immediately following it, explicit methods, on the other hand, find a solution by referring only to a time following the state of the system at the time considered. In formulas this can be expressed synthetically as:

- *Explicit Method*

$$Y(t+\Delta t) = F(Y(t)) \tag{24}$$

- *Implicit Method*

$$G(Y(t), Y(t+\Delta t) = 0 \tag{25}$$

where $Y(t)$ is the current state of the system, and $Y(t+\Delta t)$ is the state of the system at a subsequent step of time, after an infinitesimal time interval denoted by Δt.

Thus, implicit methods require additional computations and can be much more difficult to implement than explicit methods. The explicit dynamic analysis procedure is performed by the Abaqus software efficiently following many small-time intervals. A central-type integration rule is used that satisfies the dynamic equilibrium equations at the initial moment of increment, i.e., at time t. The accelerations computed at time t are used to advance the solution related to velocity at time $t+\Delta t/2$ and the solution related to displacement at time $t + \Delta t$. Performing an explicit type of dynamic analysis has several advantages. First, it is computationally more efficient for the analysis of large models with relatively short dynamic response times and for the analysis of discontinuous processes. It uses, moreover, a theory that allows the models to undergo both large and small rotations and deformations and allows the use of automatic or fixed time increment. However, the software does not allow the implementation of damage functions for materials for analysis that are not explicit, which has proved to be fundamental for a correct analysis of the model under examination.

Moreover, the obtained uniaxial compression and tension curves will be applied to perform the analysis of existing historical structures of the Campania area for which the "element deletion" function will be applied to catch the formation of cracks. Abaqus software allows the "element deletion" function, for a user defined level of damage, only for explicit models.

The experimental tests analysed can be classified as problems of quasi-static application of forces. In addition, as models become very large, the explicit procedure requires fewer system resources than the implicit procedure. Applying the explicit dynamic procedure to quasi-static problems requires some special considerations. Since a static solution is, by definition, a long-time solution, it is often computationally impractical to simulate an event in its natural time scale, which would require an excessive number of small-time increments. To obtain an economical solution, the event must be accelerated in some way. The problem is that as the event is accelerated, the state of static equilibrium evolves into a state of dynamic equilibrium in which inertial forces become more dominant. The goal is to address the process in the shortest time in which inertial forces remain insignificant.

5.2. "Cantieri" masonry

The calibration of the parameters of the regular tuff ashlar masonry has been carried out referring to [32] where the data of experimental tests carried out on various types of tuff masonry, typical of the Neapolitan and Campania area in general, are reported. The case studies have referred to "cantieri", "bozzette" and "blocchetti a filari" types, whose reference specimen has dimensions equal to 120 × 65 × 95, 100 × 55 × 86 and 120 × 42 × 88 cm, respectively. These specimens were modelled in ABAQUS (Fig. 15), where the analysis is carried out on a solid, three-dimensional model with linear hex meshes with reduced

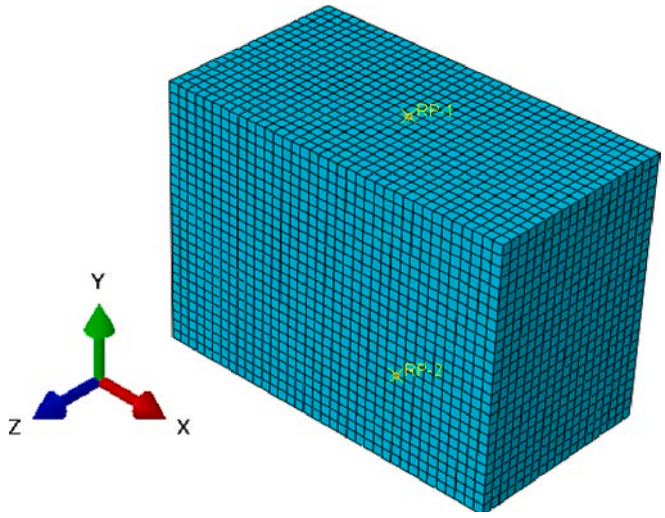

Fig. 15. Abaqus model for "Cantieri" masonry.

Table 2
Reference parameters for "cantieri", "bozzette" and "blocchetti a filari" tuff masonry.

Masonry type	σ_{max} (N/mm^2)	ε_p (%)	$\varepsilon(\sigma_{max/2})$ (%)	σ_u (N/mm^2)	ε_u (%)	E_{c0} (N/mm^2)
Cantieri (C1)	4.34	0.49	1.60	1.32	4.60	1183
Cantieri (C2)	3.60	0.88	2.40	0.72	4.00	746
Bozzette (B1)	3.32	0.55	1.78	0.66	3.10	1067
Bozzette (B2)	2.85	0.49	3.10	1.36	4.90	1252
Blocchetti a filari (S1)	2.55	0.35	1.26	0.51	3.20	923
Blocchetti a filari (S2)	2.74	0.61	1.69	0.54	2.80	743

integration (C3D8R) with the size of about 10 mm. Non-linear analysis was performed using an explicit dynamic procedure, implemented in a quasi-static manner. This type of analysis allows the use of damage parameters in compression and tension, given through a table curve, according to the theory of large deformations. The data of the tests are summarised in Table 2.

The curves resulting from the experimental tests have been compared with the curve obtained from the Abaqus software by implementing the uniaxial stresses and the damage parameters as input data. For the dilation angle parameter ψ and the flow stress ratio K, reference is made to the values suggested in [10]. The values $\psi = 20^\circ$ and $K = 0.6$ are adopted. The dilation angle is generally determined through triaxial tests or direct shear tests, and it assumes different values according to the considered material. The flow stress ratio is determined through the tensional state tests allowing to define the tensile and the compression meridians expressed in deviatoric coordinates. Since these data are not available, reference is made to [41,42,43]. According to [10], the values of ψ, start from 0° for normally consolidated clay, passing through concrete with 12° up to 20° for compact marbles. Particular types of masonry can have dilation angles of up to 30°.

Table 3
Calibration parameters for "cantieri" masonry.

Masonry type	E_0 (N/mm^2)	σ_c (N/mm^2)	ε_{c1} (–)	E_{c1} (N/mm^2)	α_a (–)	α_d (–)	ε_{yc} (–)
Cantieri (C1)	1183	4.34	0.0049	885.7	1.33	0.5	0.0029
Cantieri (C2)	746	3.6	1.08	500.1	1.492	0.59	0.001448

Moreover, in [10] a sensitivity analysis was performed. Referring to the CDP, the sensitivity analysis has highlighted that the variation of the parameters adopted for the characterization of the flow Rule (Ψ, ε, K) influences the result not as significantly as the parameters governing the curves of uniaxial tension and uniaxial compression. For all the considered masonry types, the parameter affecting the descending branch of the curve α_D showed insignificant fluctuations, ranging from 0.50 to 0.59 considering a range of variability from 0.4 to 4.00. The viscosity parameter, μ, is considered only in the standard type Abaqus analyses and not in the explicit type analyses, therefore, for the visco-plastic regularization of the constitutive equations of the material, the default value is set as equal to 0.

Consequently, to obtain reliable results, it is necessary to have models capable of adequately representing the experimental curve of the considered material, in tension and compression. Guo's model proved to be easy to use and widely adaptable in the calibration process.

Consequently, these curves have been reproduced through the Guo model [37], starting from the data provided by the experimental test and calibrating the parameters influencing the shape of the analytical curve [37–45]. The results obtained by the Abaqus software, in terms of force–displacement, have been converted, just to make a comparison, in terms of $\sigma - \varepsilon$. The results of the experimental test, in fact, are stress–strain curves, with stress (σ) provided in N/mm^2 and strain (ε) in percentage terms. The data implemented for the construction of the curves of the two tests on "cantieri" masonry are reported in Table 3. The comparison between the experimental data curve and the numerical one is reported in Fig. 16.

The data implemented for the construction of the curves of the two tests on "bozzette" masonry, are reported in Table 4. The comparison between the experimental data curve and the numerical one is shown in Fig. 17.

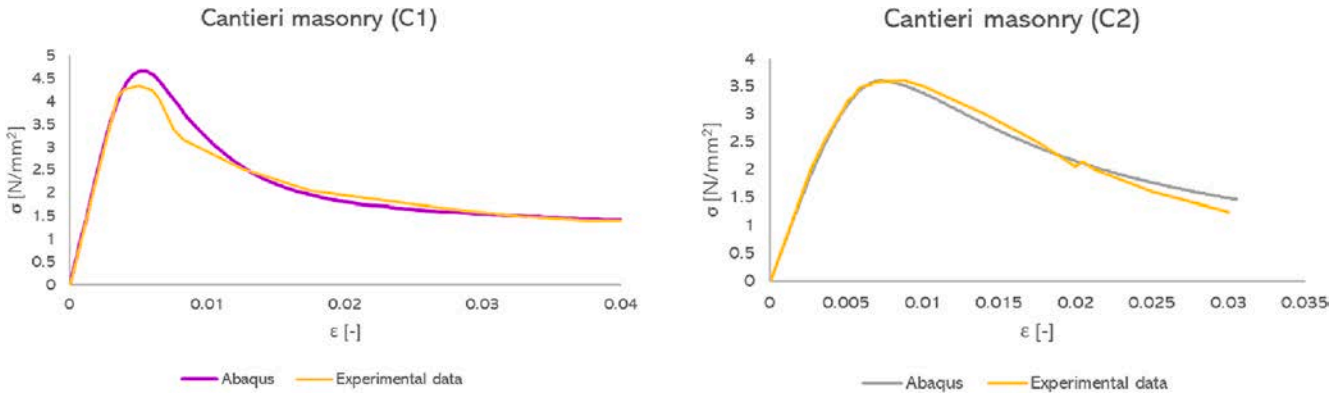

Fig. 16. Comparison between Abaqus and Experimental data curves for the "cantieri" masonry.

Table 4
Calibration parameters for "bozzette" masonry.

Masonry type	E_0 (N/mm^2)	σ_c (N/mm^2)	ε_{c1} (–)	E_{c1} (N/mm^2)	α_a (–)	α_d (–)	ε_{yc} (–)
Bozzette (B1)	1067	3.32	0.0049	677.55	1.5748	0.53	0.0009
Bozzette (B2)	1252	2.85	0.0060	475.00	2.6358	0.40	0.000683

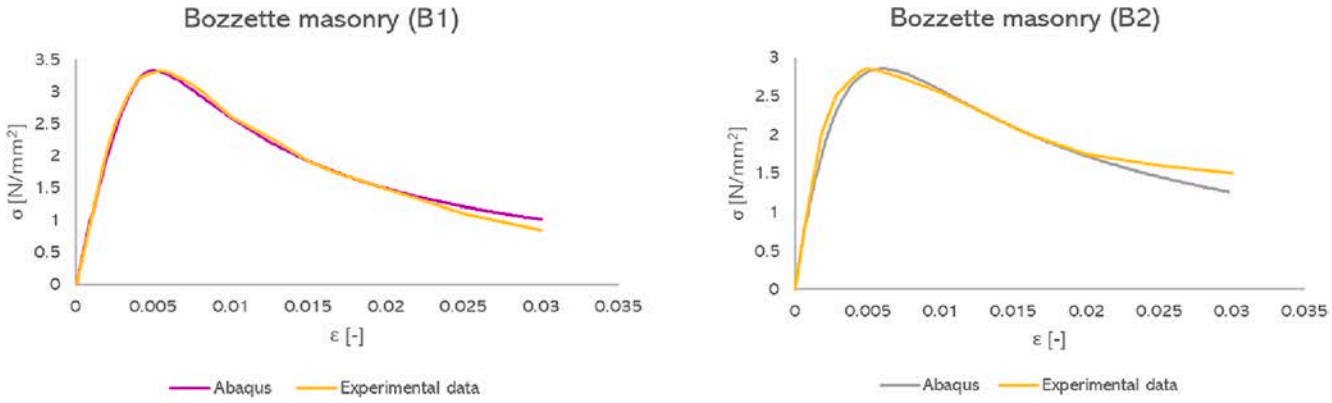

Fig. 17. Comparison between Abaqus and Experimental data curves for the "bozzette" masonry.

Table 5
Calibration parameters for "Blocchetti a filari" masonry.

Masonry type	E_0 (N/mm^2)	σ_c (N/mm^2)	ε_{c1} (–)	E_{c1} (N/mm^2)	α_a (–)	α_d (–)	ε_{yc} (–)
Blocchetti a filari (S1)	923	2.55	0.00397	643.13	1.4352	0.58	0.00083
Blocchetti a filari (S2)	743	2.74	0.0056	489.29	1.5185	0.59	0.0011

The data implemented in Excel for the construction the curves of the two tests on "blocchetti a filari" masonry, are reported in Table 5. The comparison between the experimental curve and the numerical one is reported in Fig. 18.

The perfect compliance of the results reported in Figs. 16–18 is due to the adequate modelling in ABAQUS with the Concrete Damaged Plasticity model. The details of the Stress-Strain, Stress-Inelastic Strain, Damage Parameter-Strain and Damage Parameter- Inelastic Strain curves are reported in the Appendix with reference to all the considered masonry typology.

5.3. *Simple listed masonry*

The calibration of simply listed masonry has been performed referring to an experimental test carried out at the Civil Engineering Department of the University of Cassino and Lazio Meridionale [32]. The panels have a thickness equal to 150 mm, a width equal to 610 mm, and a height variable in a range between 650 and 635 mm. In particular, the panel modelled for calibration is the simply listed masonry panel, 645 mm high. The dimensions of the ashlars are also standardized: the single ashlar of tuff has a dimension of 300 × 150 × 100 mm, while the brick has a dimension of 300 × 150 × 33 mm (Fig. 19). As in the case of the simple tuff masonry, the simple listed masonry has been modelled in Abaqus to compare the curve obtained from the software with the reference curve, obtained from the experimental test. The parameters of the materials are reported in Table 6 while the tests on the masonry have provided the compressive strength and Young's modulus reported in Table 7 [39–45]. For the dilation angle parameter ψ and the flow stress ratio K reference is made to the values suggested in [10].

The data required to construct the curves for the ABAQUS modelling are summarized in Table 8. The comparison between the two curves obtained is reported in Fig. 20.

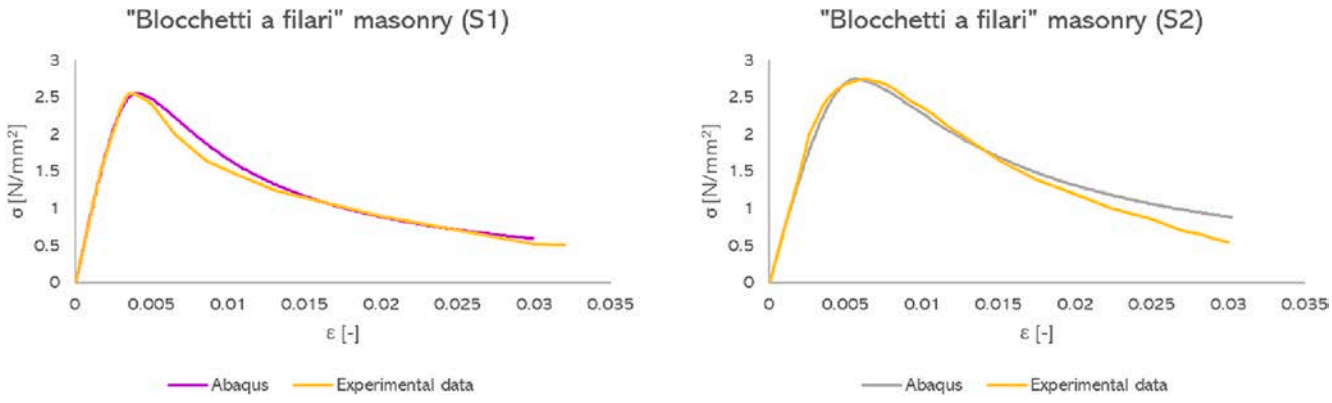

Fig. 18. Comparison between Abaqus and Experimental data for the "Blocchetti a filari" masonry.

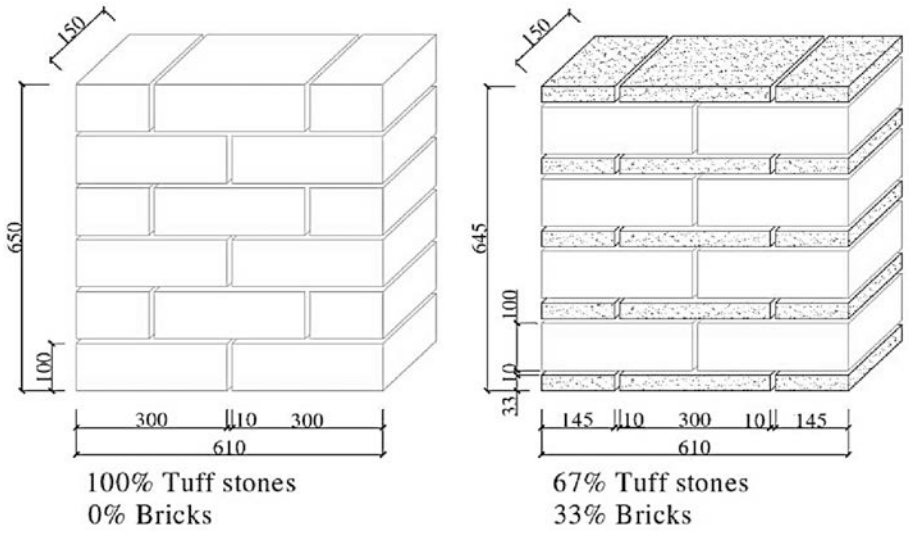

Fig. 19. Geometry of wall panels used for experimental testing.

Table 6
Experimental data parameters for single components of the masonry.

Material	Compressive strenght f_b (MPa)	Tensile strenght f_{bt} (MPa)	Young's modulus E_b (MPa)	Shear modulus G_b (MPa)
Tuff	4.13	0.24	1540	444
Bricks	25.15	4.52	16,000	–
Mortar	7.14	1.43	1520	659

Table 7
Experimental data parameters for the panels.

PANEL	Compressive strenght f_m (MPa)	Young's modulus E_b (MPa)
Simple listed	2.58	930

Table 8
Calibration parameters for simple listed masonry.

E_0 (N/mm^2)	σ_c (N/mm^2)	ε_{c1} (–)	E_{c1} (N/mm^2)	α_a (–)	α_d (–)	ε_{yc} (–)
1820	3.354	0.0014	1552.7	1.17	0.7	0.00147

6. Calibration for "shell" elements: Modelling and comparison with "brick" elements

Generally, the process of calibration on equivalent homogeneous models is the basis of modelling of very complex structures such as ancient churches, historical buildings, or towers. The use of brick elements in such complex assemblies hugely increases the computational time, therefore, the use of a reduced number of integration point as in the shell element can be favourable for the simplification of the computational process. Therefore, the comparison between the brick modelling and shell modelling for the same masonry typology investigated in the previous chapters is reported. This comparison has been carried out to understand the differences between the two types of models in terms of results, to succeed in calibrating a possible factor of scale. To reduce the operational complexity and the computational burden, the calibration process was also applied on shell type elements, first reproducing the compression tests previously exposed, then for horizontal actions on a study wall [46].

The solid model foresees the creation of three-dimensional "brick" elements of tetrahedral or quadrilateral shape. The shell elements, instead, reduce the development of the structure to its average surface. The inertial properties of the element of interest are assigned by defining

Fig. 20. Comparison between Abaqus and Experimental data curves.

the value of the thickness of the elements that form the FE model. Two types of shell elements are available in Abaqus software, namely conventional shell elements and continuous shell elements. Conventional shell elements distinguish a reference surface by defining the elements planar dimensions, its surface normal, and its initial curvature. Continuous shell elements, on the other hand, resemble three-dimensional solid elements in that they discretize an entire three-dimensional body, but are formulated so that their kinematic and constitutive behaviour is like conventional shell elements. Since shell elements are modelled in 3D but as two-dimensional elements, the timing and analysis issues are greatly reduced compared to the solid model case. In the case of compression tests, the results for "shell" and "brick" elements are perfectly overlapping for all the materials considered. An example is shown in Fig. 21 for a selection of the investigated experimental tests.

6.1. Comparison between "brick" and "shell" elements under horizontal actions

As no information are available in literature about experimental tests of the investigated masonry subjected to horizontal loads, the methodology adopted consists in applying the material models described above to the so called "Pavia wall" [46,47,48]. Good calibration results have been already obtained in a previous work [10] however, the modelling was developed by brick elements only. In this work, the Pavia Door Wall

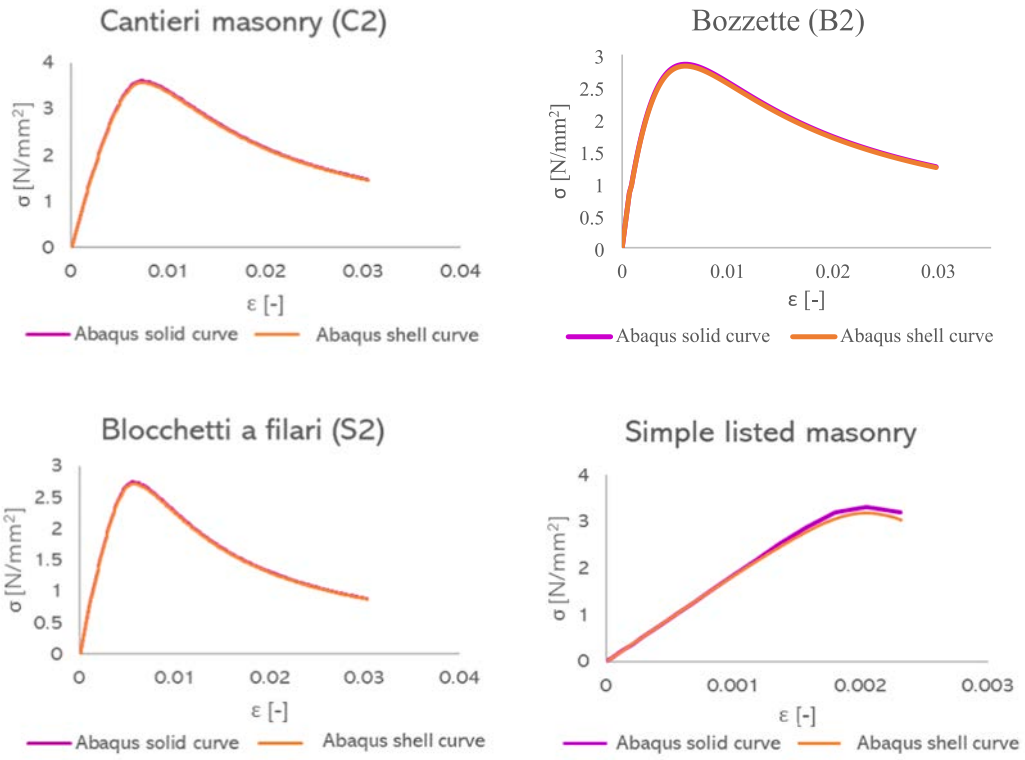

Fig. 21. Comparison between Abaqus "Solid" and "Shell" curves in compression.

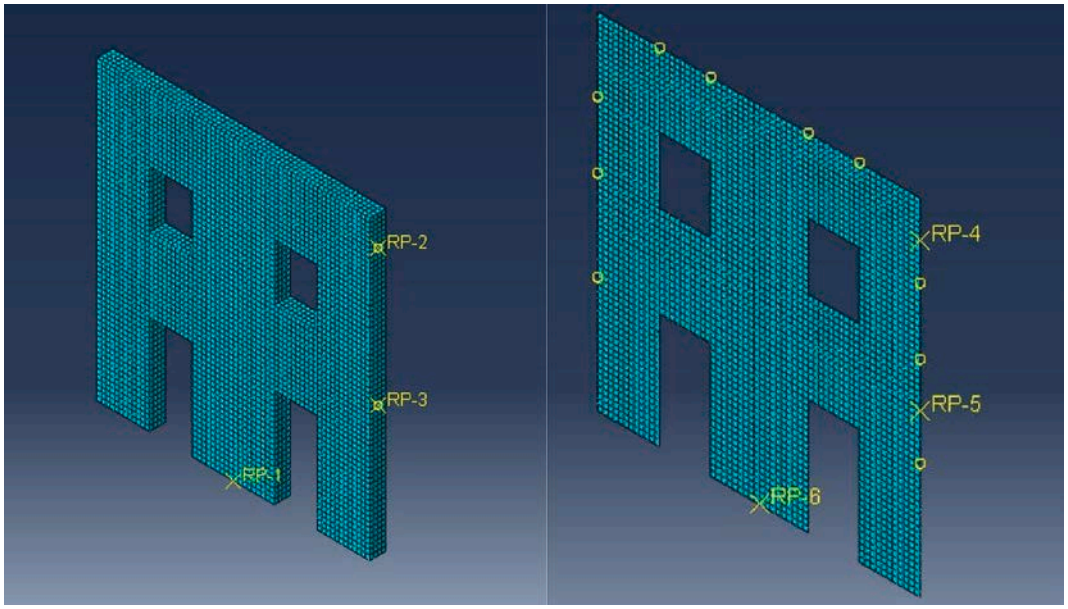

Fig. 22. Comparison between Abaqus "Solid" and "Shell" mesh pattern.

in its exact dimensions has been modelled in Abaqus [10], and with the real applied loads, going to simulate the test carried out experimentally. The analysis was conducted first by creating both three-dimensional solid brick model, and a two-dimensional shell model, to evaluate any differences between the two modelling and to be able to use a shell model, with significantly low time for analysis. With reference to the wall, in both types of models, coupling constraints have been created in correspondence of the two rigid decks and at the base. For each coupling a reference point has been chosen, successively, to which boundary conditions have been applied: at the height of the two rigid decks a boundary condition of type "displacement/rotation" has been applied, allowing the displacement only in the horizontal direction; at the base a boundary condition of encastre has been placed to not allow displacements or rotations in any direction.

Hex mesh type is chosen for both the solid model and the shell model so the meshing takes place using hexahedral elements, in the case of three-dimensional models, or quadrangular, in the case of two-dimensional models, and it is indicated for structures such as the one in question, having, therefore, regular forms. Moreover, the so called "structured" mesh is used with a regular size of about 100 mm (Fig. 22).

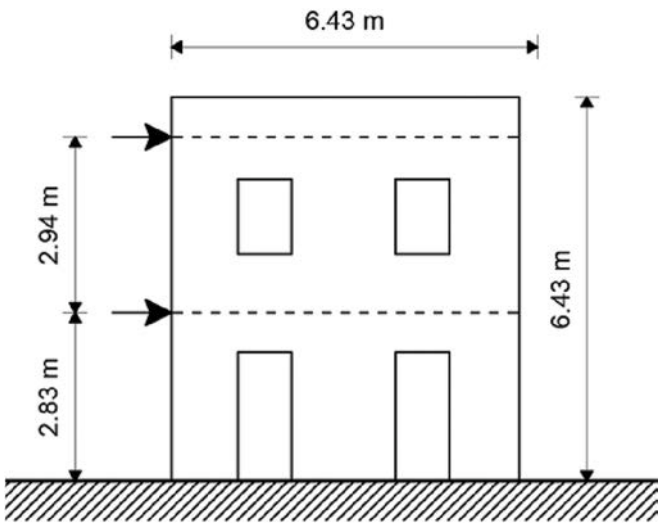

Fig. 23. Geometric scheme of the "Door Wall" in Pavia.

First, the same materials used in the experimental test of the "Pavia door wall" (Fig. 23) have been applied to both the brick and the shell model (Table 9). In Fig. 24 the curves corresponding to the brick and the shell model and the experimental curve are reported. It is observed that the brick model exactly captures the behaviour of the experimental test and at the same time the shell model is very close (Fig. 24).

After that, the procedure was applied also considering the materials discussed in this work, for which the calibration procedure for vertical actions has already been reported. The calibration for horizontal actions has been pursued first on a solid model, then also on a shell model, to verify the adherence between the results. The tests have been carried out for each type of material: both for shell and solid model the parameters of the inserted materials have been left unchanged. Reference is made to the Elastic Modulus and the uniaxial compression and tension curves. Also, the dilation angle ψ and the flow stress ratio *K*, have been left unchanged with respect to the solid model.

For each masonry typology, the curve obtained performing the analysis on a solid model (brick) and the curve obtained performing the analysis on a shell model (Figs. 25–28) are reported and it can be observed that they are perfectly overlapped. In particular, considering a value of the "top sway displacement", the corresponding "total base shear" value has a maximum deviation of 2% between the "shell" and the "solid" model (the difference increases with the plastic deformation).

7. Conclusions

In this paper, the calibration of the parameter for the detailed modelling of four typical tuff masonry systems spread in Campania region is reported. The calibration has been performed by exploiting the model proposed by Guo, based on the Concrete Damaged Plasticity model (CDP). CDP is the most suitable failure criterion for the analysis of wall panels, especially for the control of cracks, being a model in which the evolution of the failure domain and therefore of the parameters that govern its behaviour, is linked to the level of damage. The calibration carried out showed very high levels of precision. The modelling in the ABAQUS software, although simple, has led to precise results for the simulation of compression tests, as evidenced by Figs. 16–18 and Fig. 20. This result is probably linked to the possibility to catch the variation of the cohesion and the evolution of the damage given by CDP failure criterion.

Table 9
Mechanical parameters of the Pavia Door Wall.

	E [MPa]	G [MPa]	f_{wc} [MPa]	f_{vd0} [MPa]	c [MPa]	μ [−]	f_{bt} [MPa]
Masonry	1400	480	6.20	0.18			
Mortar					0.23	0.58	
Bricks							1.22

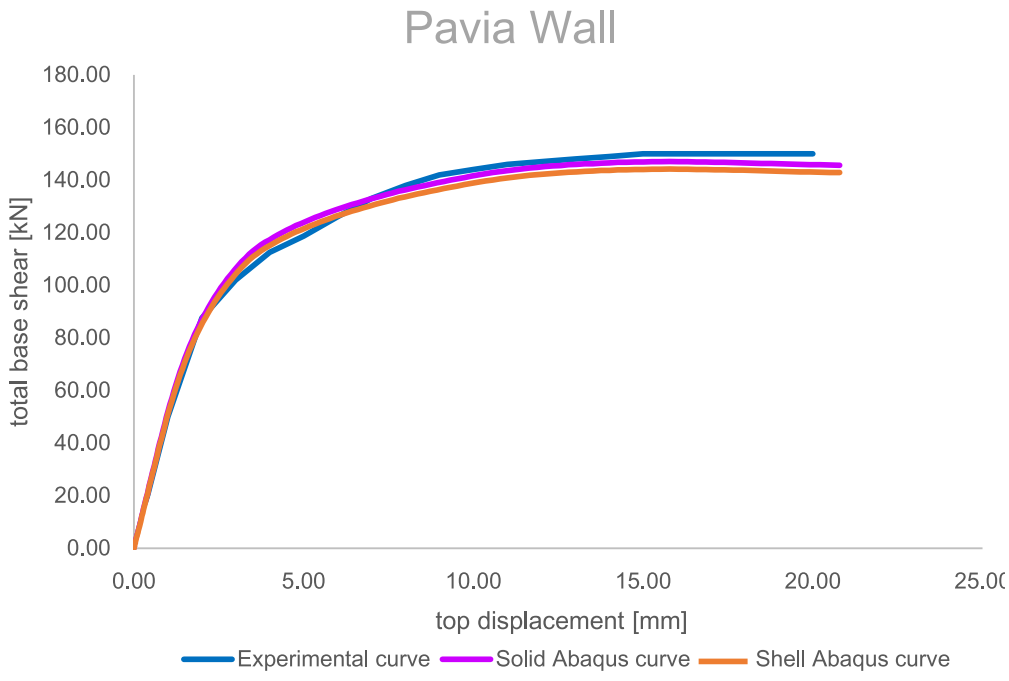

Fig. 24. Comparison between Abaqus "Solid" and "Shell" curves for "Pavia Wall" masonry in shear.

Fig. 25. Comparison between Abaqus "Solid" and "Shell" curves for simple listed masonry in shear.

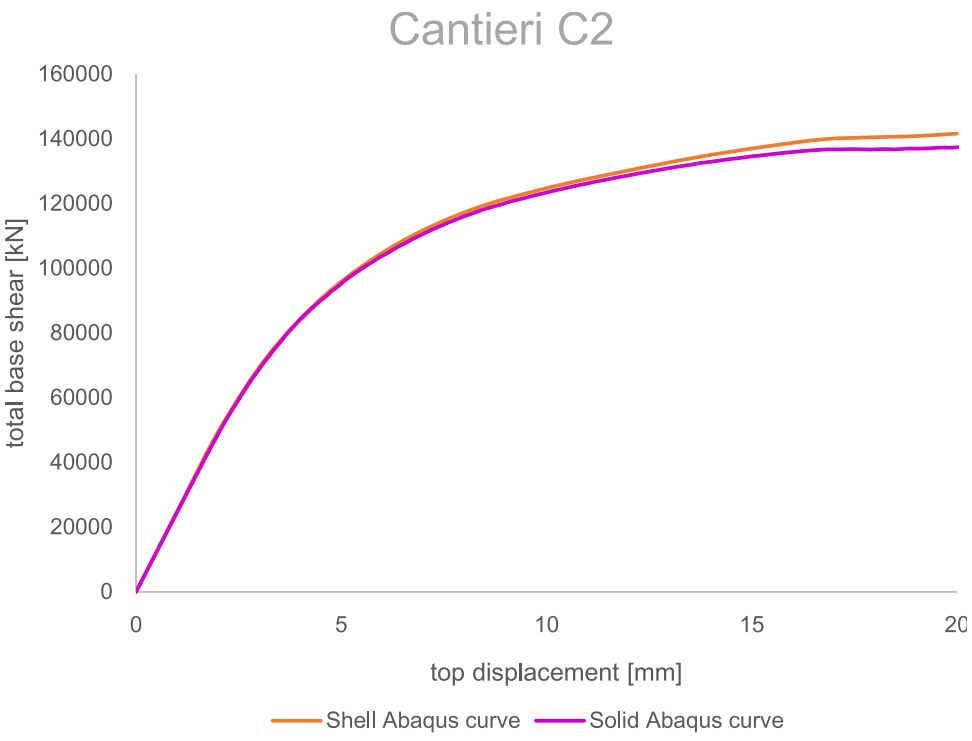

Fig. 26. Comparison between Abaqus "Solid" and "Shell" curves for "Cantieri" masonry in shear.

For the axial compression tests, the perfect adherence to the results was highlighted considering the use of "brick" elements and "shell" elements. After calibrating and defining the uniaxial behaviour of the materials, a further calibration process was conducted for the shear actions, starting from the experimental data and materials provided by [46] for the so-called "Pavia wall". The FEM analysis with both solid and shell elements showed perfect adherence with the results of the experimental test.

Subsequently, this procedure was also applied considering the materials covered in the present work. The results obtained with the shell model showed perfect adherence with those obtained through the solid model. In particular, in the comparison between the "shell" and the "solid" model, the scatter in terms of base shear force or compression stress, for a given displacement or deformation parameter, was equal to

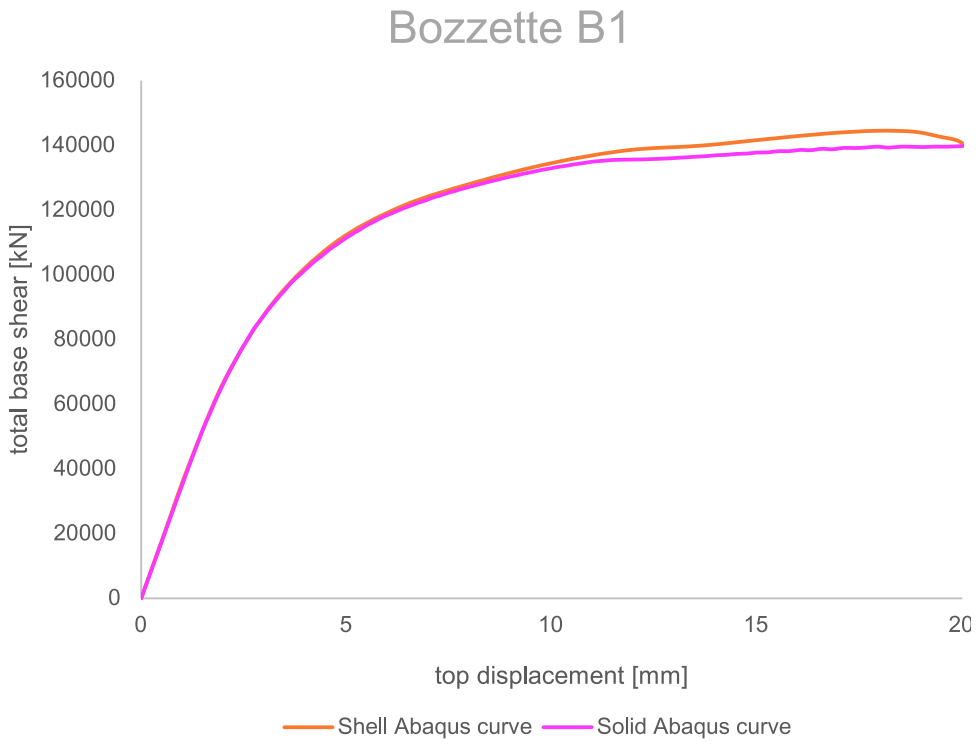

Fig. 27. Comparison between Abaqus "Solid" and "Shell" curves for "Bozzette" masonry in shear.

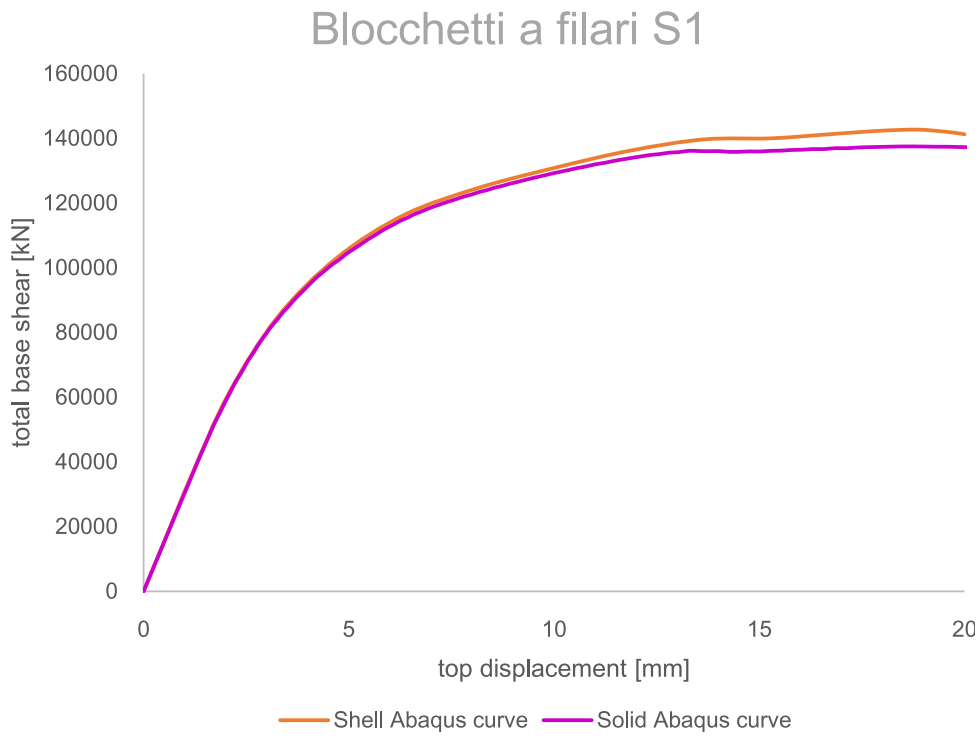

Fig. 28. Comparison between Abaqus "Solid" and "Shell" curves for "Blocchetti a filari" masonry in shear.

2% (the difference increases with the plastic deformation). With the shell model, it is possible to reduce computational efforts (in the case of horizontal pushover analyses) using the same behavioural parameters of the material used for the solid model.

In conclusion, it can be stated that the proposed model has great flexibility, and it can be calibrated on several types of masonry. The usefulness of this study is the possibility of exploiting the calibration parameters obtained for CDP failure criterion to analyse the numerous existing buildings made with the analysed materials. Downstream of the results obtained, the possibility of using a "shell" model has also been consolidated to assure a faster computation. In addition, no correction factor was found for shear actions when comparing "shell" and "brick" models.

Moreover, the obtained uniaxial compression and tension curves will be applied to perform static non-linear and dynamic non-linear analysis of existing historical structures of the Campania area.

Ethical statement

This paper has not been previously published, is not currently submitted for review to any other journal, and will not be submitted elsewhere during peer review for *Engineering Structures*.

CRediT authorship contribution statement

Elide Nastri: Conceptualization, Methodology, Validation, Resources, Data curation, Writing – review & editing, Supervision. **Michela Tenore:** Software, Methodology, Writing – original draft, Investigation, Formal analysis. **Paolo Todisco:** Software, Validation, Methodology, Writing – original draft, Investigation, Formal analysis.

Declaration of Competing Interest

The authors declare that they have no known competing financial interests or personal relationships that could have appeared to influence the work reported in this paper.

Data availability

No data was used for the research described in the article.

Appendix

See the Figs. 29–44.

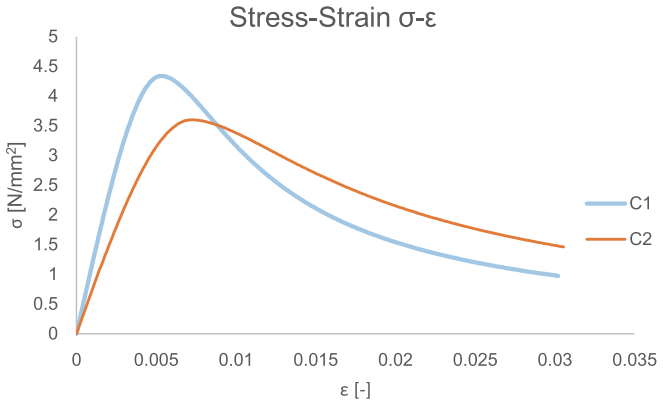

Fig. 29. Stress-Strain curve for “cantieri” masonry in compression.

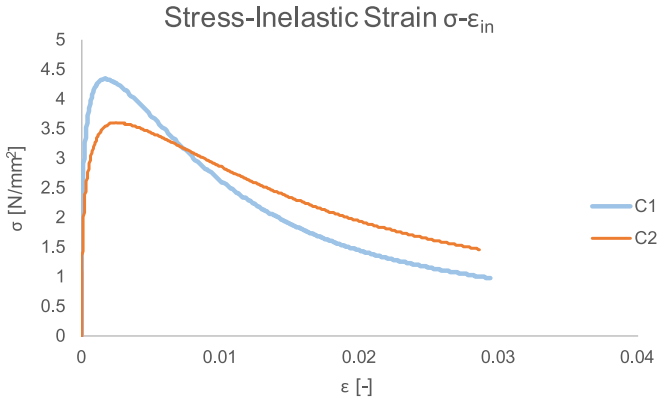

Fig. 30. Stress-Cracking strain curve for “cantieri” masonry.

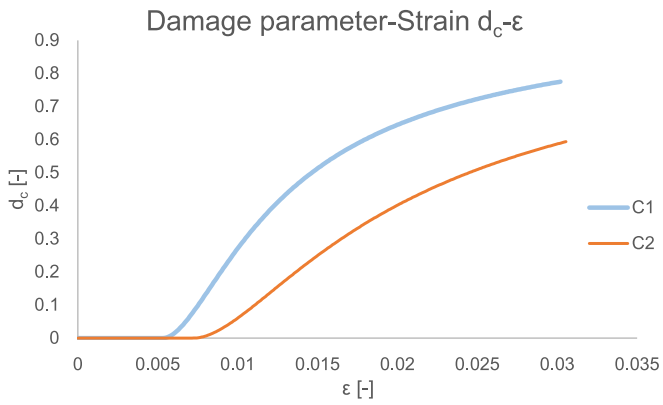

Fig. 31. Damage parameter-Strain curve for “cantieri” masonry.

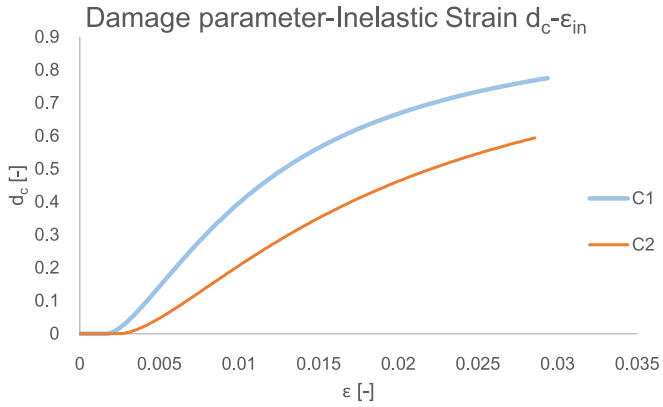

Fig. 32. Damage parameter-Inelastic strain curve for “cantieri” masonry.

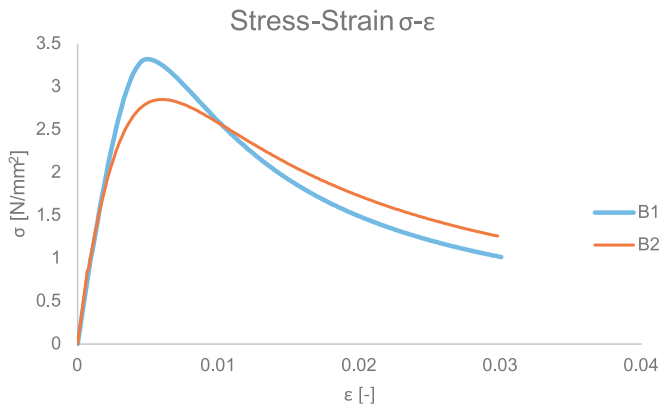

Fig. 33. Stress-Strain curve for “bozzette” masonry in compression.

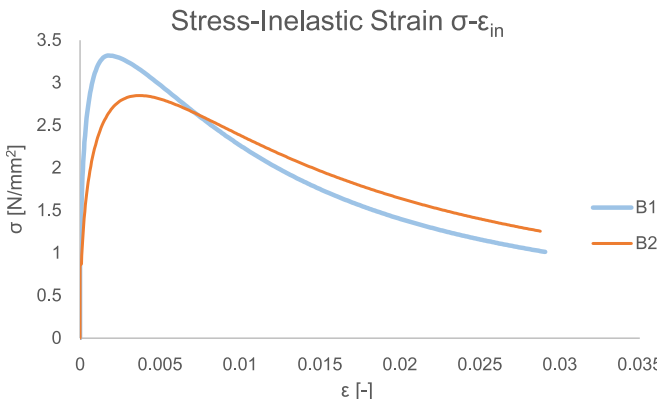

Fig. 34. Stress-Cracking strain curve for "bozzette" masonry.

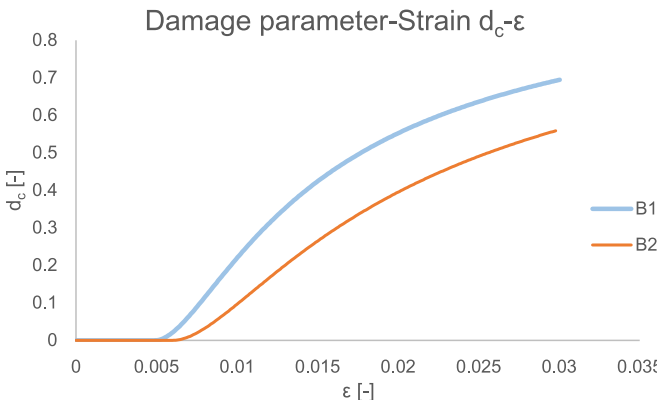

Fig. 35. Damage parameter-Strain curve for bozzette masonry.

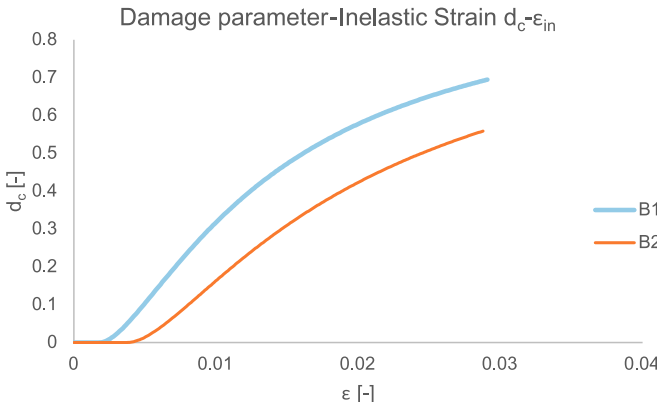

Fig. 36. Damage parameter-Inelastic strain curve for "bozzette" masonry.

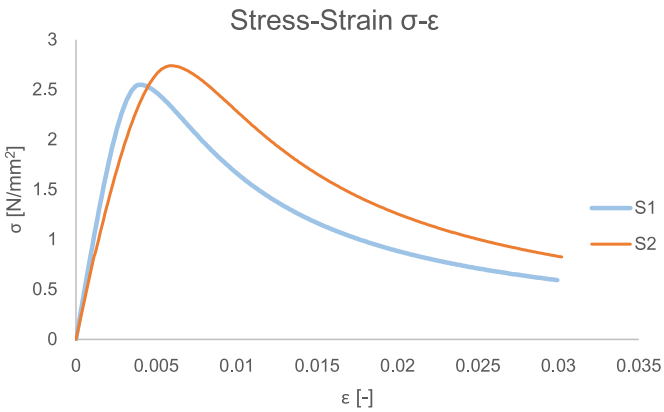

Fig. 37. Stress-Strain curve for "blocchetti a filari" masonry in compression.

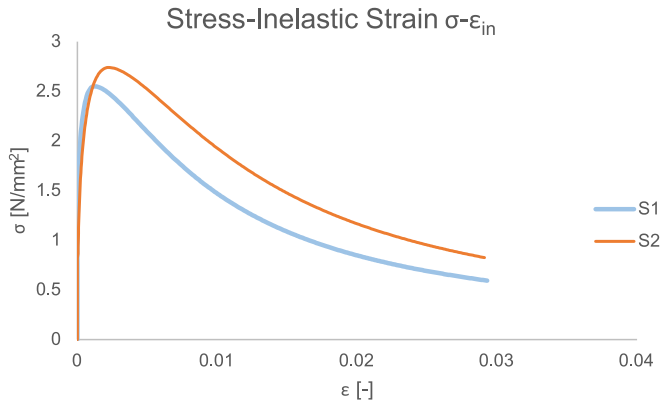

Fig. 38. Stress-Cracking strain curve for "blocchetti a filari" masonry.

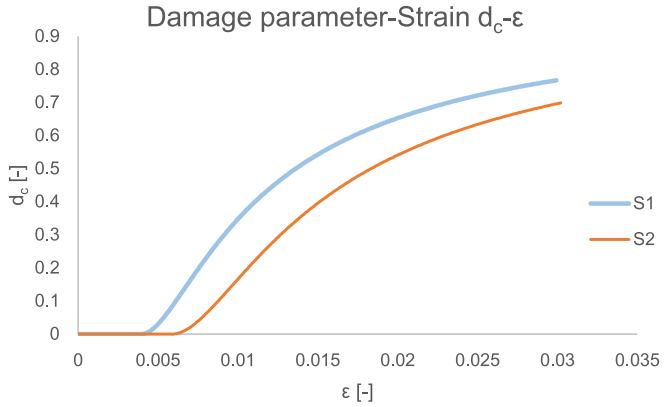

Fig. 39. Damage parameter-Strain curve for "blocchetti a filari" masonry.

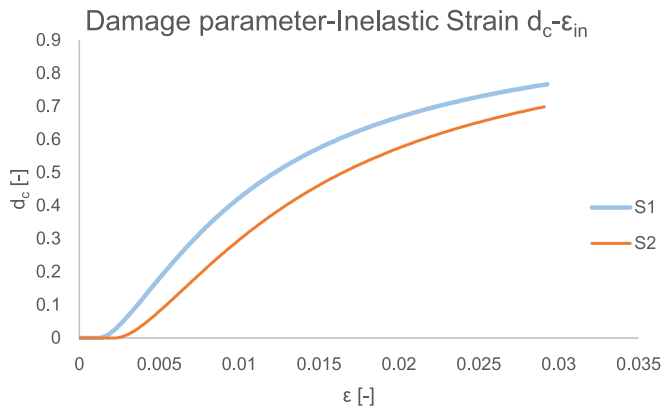

Fig. 40. Damage parameter-Inelastic strain curve for "blocchetti a filari" masonry.

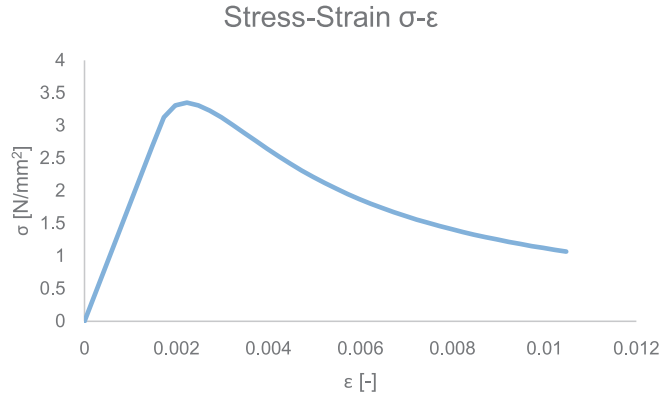

Fig. 41. Stress-Strain curve for simple listed masonry in compression.

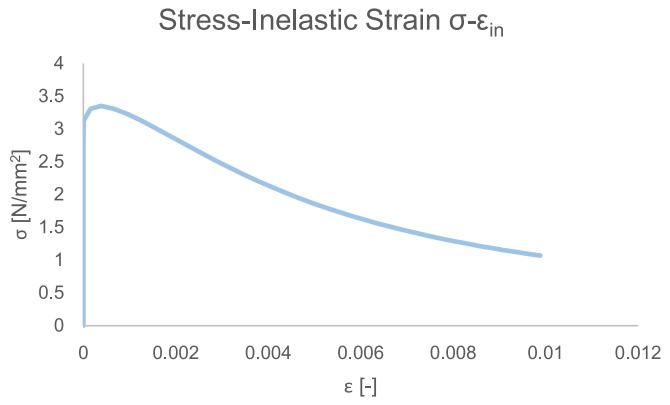

Fig. 42. Stress-Inelastic strain curve for simple listed masonry.

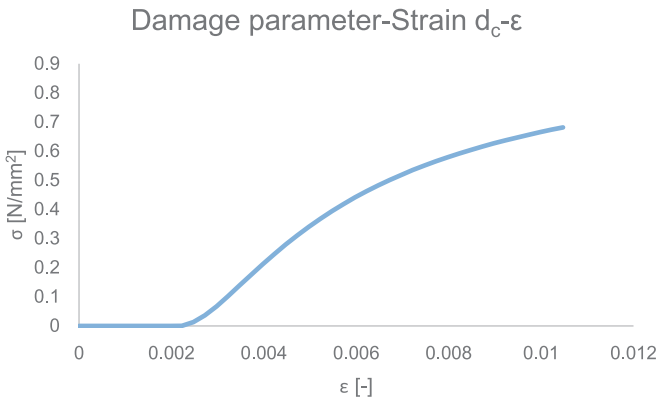

Fig. 43. Damage parameter-Strain curve for simple listed masonry.

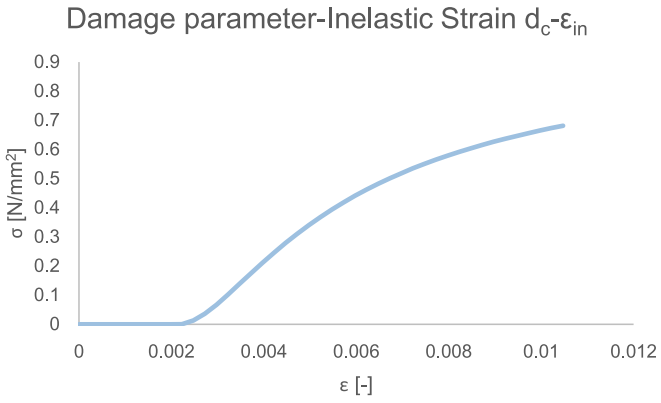

Fig. 44. Damage parameter-Inelastic strain curve for simple listed masonry.

References

[1] ISTAT 2011, "15° Censimento generale della popolazione e delle abitazioni"; 11 August 2014.

[2] Kwon YW. Revisiting Failure of Brittle Materials. J Pressure Vessel Technol, Trans ASME 2021;143(6). art. no. 4050989.

[3] Gaetano D, Greco F, Leonetti L, Lonetti P, Pascuzzo A, Ronchei C. An interface-based detailed micro-model for the failure simulation of masonry structures. Eng Fail Anal 2022;142. art. no. 106753.

[4] Yu L-L, Dong Z-Q, Li G. Simplified mechanical models for the seismic collapse performance prediction of unreinforced masonry structures. Eng Struct 2022;258. art. no. 114131.

[5] Rotunno T, Fagone M, Ranocchiai G, Grande E. Micro-mechanical FE modelling and constitutive parameters calibration of masonry panels strengthened with CFRP sheets. Compos Struct 2022;285. art. no. 115248.

[6] Petracca M, Camata G, Spacone E, Pelà L. Efficient Constitutive Model for Continuous Micro-Modeling of Masonry Structures. Int J Archit Herit 2022.

[7] Fagone M, Ranocchiai G, Rotunno T, Grande E. Predictive Capability of a Finite Element Micro-Mechanical Model for Masonry Elements Reinforced Using CFRP. Key Eng Mater 2022;916 KEM:186–92.

[8] Drougkas A, Sarhosis V. Micro-mechanical homogenisation of three-leaf masonry walls under compression. Eng Struct 2021;245. art. no. 112890.

[9] Calderón S, Sandoval C, Milani G, Arnau O. Detailed micro-modeling of partially grouted reinforced masonry shear walls: extended validation and parametric study. Arch Civ Mech Eng 2021;21(3). art. no. 94.

[10] Nastri E, Todisco P. Macromechanical Failure Criteria: Elasticity, Plasticity and Numerical Applications for the Non-Linear Masonry Modelling. art. no. 1245 Buildings 2022;12(8). https://doi.org/10.3390/buildings12081245.

[11] Drougkas A. Macro-modelling of orthotropic damage in masonry: Combining micro-mechanics and continuum FE analysis. Eng Fail Anal 2022;141. art. no. 106704.

[12] Dhir PK, Tubaldi E, Pantò B, Caliò I. A macro-model for describing the in-plane seismic response of masonry-infilled frames with sliding/flexible joints. Earthq Eng Struct Dyn 2022;51(12):3022–44.

[13] Kumar A, Pallav K. Dynamic Time History Analysis of Masonry Tower Using Macro Modelling Approach. Lecture Notes in Civil Engineering 135 LNCE 2021. p. 167–76.
[14] Milani G, Valente M, Fagone M, Rotunno T, Alessandri C. Advanced non-linear numerical modeling of masonry groin vaults of major historical importance: St John Hospital case study in Jerusalem. Eng Struct 2019;194:458–76. https://doi.org/10.1016/j.engstruct.2019.05.021. ISSN 0141–0296.
[15] Valente M. Seismic vulnerability assessment and earthquake response of slender historical masonry bell towers in South-East Lombardia. ISSN 1350–6307 Eng Failure Analy 2021;129:105656. https://doi.org/10.1016/j.engfailanal.2021.105656.
[16] Kouris LAS, Bournas DA, Akintayo OT, Konstantinidis AA, Aifantis EC. A gradient elastic homogenisation model for brick masonry. Eng Struct 2020;208. art. no. 110311.
[17] Liu G-Y, Xu W-J, Zhou Q, Zhang X-L. Contact Overlap Calculation Algorithms and Benchmarks Based on Blocky Discrete-Element Method. Int J Geomech 2022;22(12). art. no. 04022227.
[18] Clementi F, Milani G, Ferrante A, Valente M, Lenci S. Crumbling of Amatrice clock tower during 2016 Central Italy seismic sequence: Advanced numerical insights. Frattura ed Integrità Strutturale 2019;14(51):313–35. https://doi.org/10.3221/IGF-ESIS.51.24.
[19] Azevedo NM, Pinho FFS, Cismaşiu I, Souza M. Prediction of Rubble-Stone Masonry Walls Response under Axial Compression Using 2D Particle Modelling. Buildings 2022;12(8). art. no. 1283.
[20] Occhipinti G, Caliò I, D'Altri AM, Grillanda N, de Miranda S, Milani G, et al. Nonlinear finite and discrete element simulations of multi-storey masonry walls. Bull Earthq Eng 2022;20(4):2219–44.
[21] Castellazzi G, Pantò B, Occhipinti G, Talledo DA, Berto L, Camata G. A comparative study on a complex URM building: part II—issues on modelling and seismic analysis through continuum and discrete-macroelement models. Bull Earthq Eng 2022;20(4):2159–85.
[22] De Iasio A, Wang P, Scacco J, Milani G, Li S. Longhu pagoda: Advanced numerical investigations for assessing performance at failure under horizontal loads. Eng Struct 2021;244. art. no. 112715.
[23] Malena M, Genoese A, Panto B, Spina D, de Felice G. Two Steps Procedure for the Finite Elements Seismic Analysis of the Casamari Gothic Church. art. no. 1451 Buildings 2022;12(9). https://doi.org/10.3390/buildings12091451.
[24] Yavartanoo F, Kang T-H-K. Dry-Stack Masonry Wall Modeling Using Finite-Element Method. art. no. 04022176 J Struct Eng (United States) 2022;148(11). https://doi.org/10.1061/(ASCE)ST.1943-541X.0003457.
[25] Pantò B, Grosman S, Macorini L, Izzuddin BA. A macro-modelling continuum approach with embedded discontinuities for the assessment of masonry arch bridges under earthquake loading. art. no. 114722 Eng Struct 2022;269. https://doi.org/10.1016/j.engstruct.2022.114722.
[26] Malcata M, Ponte M, Tiberti S, Bento R, Milani G. Failure analysis of a Portuguese cultural heritage masterpiece: Bonet building in Sintra. Eng Fail Anal 2020;115. art. no. 104636.
[27] Formisano A, Chieffo N, Mosoarca M. Seismic vulnerability and damage speedy estimation of an urban sector within the municipality of San Potito Sannitico (Caserta, Italy). Open Civ Eng J 2017;11:1106–21. https://doi.org/10.2174/1874149501711011106.
[28] Chieffo N, Formisano A. Geo-hazard-based approach for the estimation of seismic vulnerability and damage scenarios of the old city of senerchia (Avellino, Italy). art. no. 59 Geosciences (Switzerland) 2019;9(2). https://doi.org/10.3390/geosciences9020059.
[29] Chieffo N, Formisano A. The influence of geo-hazard effects on the physical vulnerability assessment of the built heritage: An application in a district of Naples 2019;9 (1), art. no. 26, Doi: 10.3390/buildings9010026.
[30] Marghella G, Marzo A, Carpani B, Indirli M, Formisano A. Comparison between in situ experimental data and Italian code standard values(2016) Brick and Block Masonry: Trends, Innovations and Challenges - Proceedings of the 16th International Brick and Block Masonry Conference, IBMAC; 2016. p. 1707–1714. Doi: 10.1201/b21889-212.
[31] Calderoni B, Cecere G, Cordasco EA, Guerriero L, Lenza P, Manfredi G. Metrological definition and evaluation of some mechanical properties of post-medieval Neapolitan yellow tuff masonry. J Cult Herit 2010;11(2):163–71.
[32] Grande E, Romano A. Experimental investigation and numerical analysis of tuff-brick listed masonry panels. Mater Struct/Materiaux et Construct 2013;46(1–2):63–75.
[33] Noor-E-Khuda S. An Explicit Finite-Element Modeling Method for Masonry Walls Using Continuum Shell Element. J Arch Eng 27(4), art. no. 04021040.
[34] Abaqus Theory Material and Documentation, Version 6.6, 6.7, 6.11.
[35] Lee J, Fenves GL. Numerical implementation of plastic damage model for concrete under cyclic loading: Application to concrete dam. Rep. No. UCB/SEMM-94/03, Department of Civil Engineering, University of California, Berkeley, Calif; 1994.
[36] Lubliner J, Oliver J, Oller S, Oñate E. A plastic-damage model for concrete. Int J Solids Struct 1989;25(3):299–326.
[37] Guo Z. Principles of Reinforced Concrete. 1st ed. Oxford, Elsevier; 2014. 587 f.
[38] Santos CFR, Alvarenga RCSS, Ribeiro JCL, Castro LO, Silva RM, Santos AAR, et al. research article "Numerical and experimental evaluation of masonry prisms by finite element method". Brasil: Escola de Engenharia de São Carlos; 2017.
[39] Sousa R, Guedes J, Sousa H. Characterization of the uniaxial compression behaviour of unreinforced masonry-Sensitivity analysis based on a numerical and experimental approach. Arch Civ Mech Eng 2015;15(2):532–47. https://doi.org/10.1016/j.acme.2014.06.007.
[40] Le Minh H, Khatir S, Wahab MA, Cuong-Le M. A concrete damage plasticity model for predicting the effects of compressive high-strength concrete under static and dynamic loads. ISSN 2352–7102 J Build Eng 2021;44:103239. https://doi.org/10.1016/j.jobe.2021.103239.
[41] Shakor P, Gowripalan N, Rasouli H. Experimental and numerical analysis of 3D printed cement mortar specimens using inkjet 3DP. Arch Civ Mech Eng 2021;21:58.
[42] Chen WF, Han DJ. Plasticity for Structural Engineers. Fort Lauderdale, FL, USA: J. Ross Publishing Inc; 2007.
[43] Kwon YW. Revisiting Failure of Brittle Materials. J Press Vessel Technol 2021;143:4050989.
[44] EN 1996 – 1 - Eurocode 6 - Design of masonry structures (part 1.1).
[45] EN 1996 – 1 - Eurocode 6 - Design of masonry structures (part 1.2).
[46] Abrams PDP, Calvi GM. Proceedings of the U.S.-Italian Workshop on Guidelines for Seismic Evaluation and Rehavilitation of Unreiforced Masonry Buildings; Technical Report. Pavia, Italy: University of Pavia; 1994.
[47] Rizzano G, Sabatino R, Torello G. Un nuovo modello a telaio equivalente per l'analisi statica non lineare di pareti in muratura. Fisciano: Università degli Studi di Salerno; 2011.
[48] Cattari S, Camilletti D, Magenes G, et al. Analisi di strutture benchmark per la valutazione dell'affidabilità di codici di calcolo sismico degli edifici in muratura. ANIDIS Pistoia: Università degli Studi di Genova e Università degli Studi di Pescara; 2017.